AD-A119 197 SCIENCE APPLICATIONS INC MCLEAN VA F/G 20/4
ENERGY RELEASE FROM CONDENSED PHASE MATERIALS AND HETEROGENEOUS--ETC(U)
JUL 82 K KAILASANATH, E HYMAN N00014-81-C-2418
UNCLASSIFIED SAI-83-831-WA SBI-AD-E001 333 NL

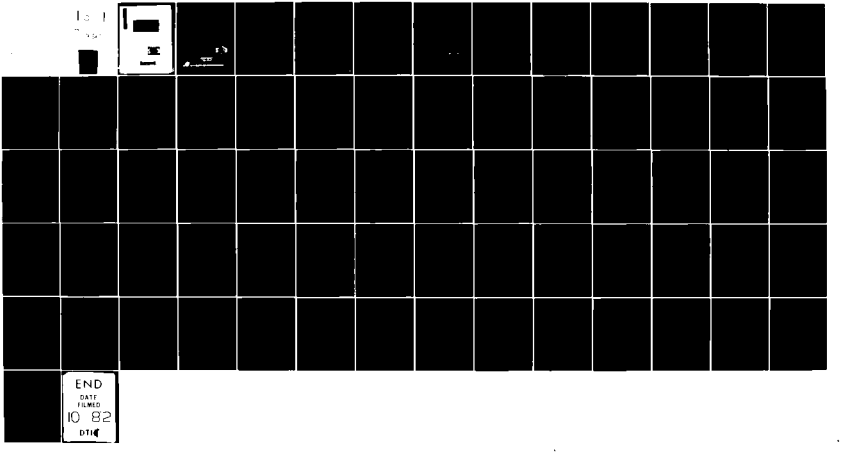

END
DATE FILMED
10 82
DTIC

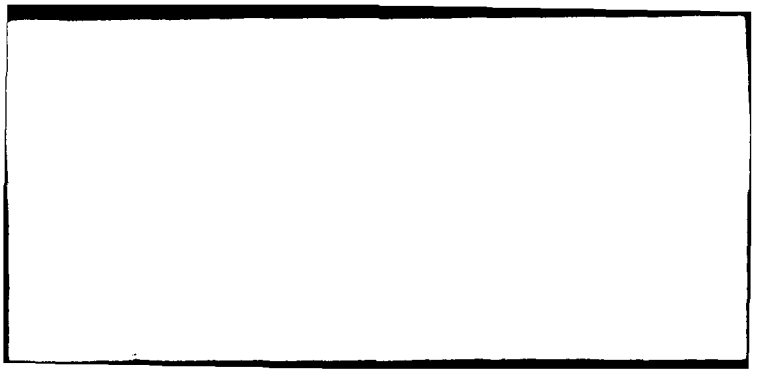

ENERGY RELEASE FROM CONDENSED PHASE MATERIALS AND HETEROGENEOUS REACTIVE FLOW MODELING

FINAL REPORT

SAI-83-831-WA

Prepared by

Kazhikathra Kailasanath and Ellis Hyman

ENERGY RELEASE FROM CONDENSED PHASE MATERIALS AND HETEROGENEOUS REACTIVE FLOW MODELING

SAI-83-831-WA

Final Report

Submitted to:

Laboratory for Computational Physics
Naval Research Laboratory
Washington, D.C. 20375

Prepared Under

Contract No. N00014-81-C-2418

Prepared by

Kazhikathra Kailasanath
and
Ellis Hyman

SCIENCE APPLICATIONS, INC.

1710 Goodridge Drive, P.O. Box 1303
McLean, Virginia 22102
(703) 734-5840

SECURITY CLASSIFICATION OF THIS PAGE (When Data Entered)

REPORT DOCUMENTATION PAGE	READ INSTRUCTIONS BEFORE COMPLETING FORM
1. REPORT NUMBER	2. GOVT ACCESSION NO. AD-A119 197	3. RECIPIENT'S CATALOG NUMBER
4. TITLE (and Subtitle) ENERGY RELEASE FROM CONDENSED PHASE MATERIALS AND HETEROGENEOUS REACTIVE FLOW MODELING	5. TYPE OF REPORT & PERIOD COVERED Final Report 18 Jun 81 - 17 Jun 82
	6. PERFORMING ORG. REPORT NUMBER
7. AUTHOR(s) Kazhikathra Kailasanath and Ellis Hyman	8. CONTRACT OR GRANT NUMBER(s) N00014-81-C-2418
9. PERFORMING ORGANIZATION NAME AND ADDRESS Science Applications, Inc. 1710 Goodridge Drive McLean, VA 22102	10. PROGRAM ELEMENT, PROJECT, TASK AREA & WORK UNIT NUMBERS
11. CONTROLLING OFFICE NAME AND ADDRESS Naval Research Laboratory 4555 Overlook Avenue, S.W. Washington, D.C. 20375	12. REPORT DATE July 1982
	13. NUMBER OF PAGES
14. MONITORING AGENCY NAME & ADDRESS(if different from Controlling Office)	15. SECURITY CLASS. (of this report) UNCLASSIFIED
	15a. DECLASSIFICATION/DOWNGRADING SCHEDULE

16. DISTRIBUTION STATEMENT (of this Report)

DISTRIBUTION STATEMENT A
Approved for public release;
Distribution Unlimited

17. DISTRIBUTION STATEMENT (of the abstract entered in Block 20, if different from Report)

18. SUPPLEMENTARY NOTES

19. KEY WORDS (Continue on reverse side if necessary and identify by block number)

Energy Release
Flames
Detonations
Reactive Flow
Droplet Combustion

20. ABSTRACT (Continue on reverse side if necessary and identify by block number)

This report describes the results from investigations on (1) the burning velocity of hydrogen in air, (2) the direct initiation of detonations in hydrogen-air mixtures and (3) the flow in and about fuel droplets.

A time dependent numerical model has been used to simulate a flame propagating in a stoichiometric hydrogen-air mixture.
(Continues)

20. Abstract (Continued)

The burning velocity of hydrogen in air was estimated from the numerical simulations and was found to be within the observed range of experimental values. The effect of inaccuracies in the estimation of the molecular diffusion coefficients and in the initial conditions have also been discussed.

Numerical simulations of shock tube experiments have been used to show that a minimum energy, a minimum power and some relation between them is required to characterize the direct initiation of detonations. These simulations also show that under certain conditions, the induction time of the gaseous mixture studied is very sensitive to perturbations in pressure and temperature. Simulations have been carried out to evaluate the effects of sound wave perturbations which in turn result in temperature and pressure fluctuations. The results of these sound wave studies show how the ignition time is affected by sound waves of a given amplitude and frequency.

The initial results from numerical simulations of the inviscid, incompressible flow in and about a non-reacting fuel droplet have also been presented.

TABLE OF CONTENTS

I. GENERAL DISCUSSION

During this contract year we have performed a number of computer simulations to investigate (1) the burning velocity of hydrogen in air, (2) the direct initiation of detonations in hydrogen-air mixtures, and (3) compressible flow around fuel droplets. The efforts and accomplishments in each of these areas will be described in some detail in the following paragraphs.

We estimated the burning velocity of hydrogen in air using a time dependent model for a flame burning in a hydrogen-oxygen-nitrogen mixture, and compared our results with experimental data. In the past,[1] SAI, in collaboration with NRL has used the NRL 1D flame code to study the ignition and quenching of flames in pre-mixed gases. The flame code has now been extended to study the propagation of laminar flames in pre-mixed gases. It was found that the time-dependent flame model is capable of predicting both the transient and steady state properties of laminar flames in hydrogen-oxygen-nitrogen mixtures. The code was used to estimate the burning velocity of hydrogen in air and this has been compared with experimental data.

The burning velocity of H_2 in air at 1 atm pressure and 298^{o}K predicted by the model was at the lower end of the observed range of experimental values. We note, however, that there are several factors which would tend to

increase this estimated value. First, the calculated burning velocity would be larger if the velocity of the unburned gas used in this calculation was closer to the flame front instead of at the open boundary. It is not clear where it should be evaluated. Second, thermal diffusion effects have not been considered in the model. Finally, the extremely important hydrogen diffusion coefficients are not really known at high temperatures. If they are higher than the ones used here, the flame velocity would increase. These observations lead us to believe that the higher observed values of the burning velocity are probably more accurate.

This study has also brought out the importance of initial conditions. As in steady-state calculations, a better initial guess leads to faster convergence to a steady propagating flame. Perhaps the best way to initialize such a problem is to perform a two step process in which we first determine the minimum ignition energy for a given radius and time of energy deposition (as reported in Ref. 1), and then deposit this energy and evaluate the properties of the propagating flame front. However, considering that the experimental velocities vary by ~25%, a good initial guess for the temperatures and species concentrations certainly gives an adequate estimate. Finally, we note that the criterion on which to judge the initial guess values is to look at how flat the

temperature profile is behind the flame front. A bad guess produces some structure and oscillations which only slowly disappear. This work has been presented at the "GAMM-Workshop on Numerical Methods in Laminar Flame Propagation" and appears in this report as Appendix A entitled, "Time-Dependent Simulation of Flames in Hydrogen-Oxygen-Nitrogen Mixtures." It will appear in the Proceedings of the GAMM-Workshop on Numerical Methods in Laminar Flame Propagation, Volume 6, in the series Notes on Numerical Fluid Dynamics.

To investigate the direct initiation of detonations in hydrogen-air mixtures we performed numerical simulations of shock tube experiments. Whereas these simulations qualitatively agree with earlier experimental observations[2,3] in that a minimum power, a minimum energy and some relation between them is required to characterize the direct initiation of detonations, the experiments and calculations do not agree well quantitatively. During the course of this study, it was found that the disagreement is primarily because the induction times of the gaseous mixtures, at the temperatures and pressures expected behind the incident shocks, are very sensitive to perturbations in pressure and temperature.

Simulations were carried out to evaluate the effects of sound wave perturbations which in turn result

in temperature and pressure fluctuations. The results of these sound wave studies showed how the ignition time is affected by sound waves of a given amplitude and frequency. It was observed that low frequency perturbations (~480 Hz or half wavelength L ~ 75 cm) of large enough amplitude (~200 m/s) can reduce the ignition time by an order of magnitude. It was found that low frequency perturbations were more likely than high frequency perturbations to cause the observed discrepancies between the experiments and calculations.

The presence of temperature and pressure variations in the experiments can be due to factors such as the non-ideal break-up of the diaphragm, boundary layers causing non-uniformities in the walls of the tube, the sudden change in shape and area of cross-section between the driver and driven sections, or heat loss to the walls. However, perturbations required to substantially alter the ignition times and cause discrepancies such as observed here are larger than what might normally be present in very well controlled shock tube experiments. This needs to be investigated before one can confidently use shock tube studies to determine the critical conditions necessary to characterize the direct initiation of detonations.

A detailed report of this study is enclosed as Appendix B. This report which is to be submitted for

publication, is entitled, "Direct Initiation of Gaseous Detonations in Shock Tubes: Numerical Simulations of Experiments."

SAI in cooperation with NRL has initiated the development of a reactive flow Lagrangian triangular grid hydrodynamic code to treat the problem of compressible flows past deformable droplets. This development began by modifying SPLISH, a Lagrangian triangular code for incompressible fluid flow in two dimensional Cartesian geometry. This code had previously been used to study Rayleigh-Taylor instabilities and flows past solid objects. Our initial modification was to convert the solid object to a denser fluid by tessalating the object and then allowing the code to treat the object as a fluid of differing density. The triangular grid allows us to place sides to triangles to approximate the droplet fluid interface while the Lagrangian nature allows us to track these interfaces while the droplet deforms in a background flow.

A typical calculation of this type is shown in figures 1 and 2. For this calculation a flow from left to right is initialized by a pressure pulse at the left boundary. For all later times the right and left sides are subjected to periodic boundary conditions. The droplet density to background fluid density ratio for this run is 2.

Figure 1 shows the triangular mesh at several times during the calculation. Early in the calculation we

see fluid flows typical of flows past solid objects. A recirculation zone forms in the wake of the droplet. The droplet eventually compresses in the direction of the flow and is forced out normal to the flow. The shear flow then pulls the top and bottom of the droplet around the recirculation zone. As the droplet thins around this recirculation zone it begins to break into several smaller pieces. Figure 2 shows the pathlines of the vertices for this same calculation. Subtracting the mean flow would show a large recirculating double vortex. Calculations with larger mass ratios show similar behavior except that the larger inertia of the droplet makes the shearing around the recirculation zone more difficult.

In order to get closer to more realistic flows we have produced and are currently testing an algorithm to simulate surface tension effects. Now, the finite difference formulae used by SPLISH for the hydrodynamics obey the conservation laws associated with the differential equations. We have formulated the surface tension forces as the gradient of a "potential" which acts only at the interface. In this way we can ensure that the finite difference algorithms will still be conservative.

The surface tension potential is given by Laplace's formula for the jump in pressure across an interface

$$P_i - P_o = \sigma/R$$

where P_i is the pressure just inside the droplet at the interface, P_o is the pressure just outside the droplet at the interface, σ is the surface tension coefficient associated with the two media which define the interface and R is the radius of curvature of the cylindrical droplet. The radius of curvature is positive at points on the interface where the droplet surface is convex and negative when the surface is concave. These pressure jumps are included in the Poisson equation for the pressure. The average pressure, $(P_i+P_o)/2$, is computed at an interface vertex. From the average pressure and the pressure jump we can compute a pressure gradient centered on triangles for inclusion in the *momentum* equation.

The radius of curvature is computed from a parametric cubic spline interpolant to the interface vertices. The parameter is a pseudo-arc length, s, defined by the Spline Knots

$$s_1 = 0$$

$$s_i = s_{i-1} + |\vec{r}_i - \vec{r}_{i-1}| \qquad i = 2, \ldots, N$$

where $\vec{r}_i$, $i = 1, \ldots, N$ are the N vertices which define the interface with $\vec{r}_N = \vec{r}_1$. The curvature is then defined by

$$K \equiv |1/R| = \frac{|(\vec{r}' \times \vec{r}'') \cdot \hat{e}_z|}{(\vec{r}' \cdot \vec{r}')^{3/2}}$$

where the prime indicates differentiation with respect to the parameter s. The sign of R at an interace, $\vec{r}_i$, is given by the sign of $(\vec{r}_{i+1} - \vec{r}_i) \times (\vec{r}_i - \vec{r}_{i-1}) \cdot \hat{e}_z$ where $\hat{e}_z$ is the unit vector in the z direction (the direction normal to the interface).

We have tested this algorithm by computing the period of a droplet undergoing oscillations due to surface tension forces. In typical runs we found periods that were approximately 15% larger than those predicted by linear theory. Similar errors were found for Rayleigh-Taylor oscillations and decreased with more refined meshes.

These results were reported on at the Eastern States Combustion Meeting in Pittsburgh, PA in October 1981. An abstract of that paper follows:

> Calculations of Flow in and About Fuel Droplets, M.J. Fritts, D.E. Fyfe*, and E.S. Oran, Naval Research Laboratory. Spray combustion is complicated by a particularly rich variety of physical processes which take place over a wide range of space and time scales. One of the important aspects of the problem is the individual and collective behavior of burning droplets. However, including the detailed interactions between droplets and the external flow field into combustion models greatly increases the computational complexity. To reduce the cost of these calculations approximations must be made that are particularly severe. The important assumptions[1,2] fall into two major areas: those concerned with droplet behavior and those concerned with the details of the external flow field.
>
> *Science Applications, Inc.

The shape of the droplets in spray combustion models are typically assumed to be spherical, and empirical expressions are used to account for drag and convection. Since the droplets are known to deform, an equivalent sphere is used to approximate the assumed deformation. The effects of droplet breakup are included by using estimated breakup times and drop sizes after breakup.

Similar assumptions are made concerning the flow about the droplets. Typically the flow is considered to be quasisteady. Thus the alteration of the flow field due to deformations and wake effects are neglected, as is the interaction of the flow field back onto the droplet. Lack of knowledge about the flow field extends to larger scales as well: in most models the droplet concentration is assumed to be dilute since little is known about droplet-droplet or droplet-wake interactions. Furthermore, the influence of transport in the external flow is based solely on ambient properties because coherent or turbulent features pose too large a complication.

Once these basic assumptions about the droplet and exterior flow have been invoked, other restrictions result because of the lack of information about the detailed flow fields both internal and external to the droplet. For example, transport properties within the drop can be treated in limiting cases only, chemical reactions are neglected in the liquid phase and in the exterior flow field, the properties of the flow field are assumed to be constant at each instant in time with only concentration diffusion considered, and pressure is assumed constant and equal to the local ambient pressure.

In this presentation we will describe the results of a new research program aimed at providing some understanding of the behavior of the internal and external flow fields in droplet combustion problems. One goal of the program is to help clarify the utility and appropriateness of some of the assumptions listed above. The program is centered on a conservative, Lagrangian description of the combustion process. This is for several reasons.[3] First, the hydrodynamics becomes simpler in that material boundaries evolve naturally and are followed without further approximations. If the method conserves vorticity as well, these material boundaries will be convected properly by any coherent vortex patterns which evolve

in the external flow field. Second, calculations of the combustion processes themselves become simpler, since local fluid parcels are followed self-consistently through their changing environment. The size of heat release in the flow field is easily determined locally, as are its effects on neighboring fluid elements. Third, several numerical advantages are incurred, such as elimination of the need to difference advective terms and the elimination of numerical diffusion resulting from lack of knowledge of interface positions.

The Lagrangian treatment used in the program is based on a finite difference treatment using an irregular, dynamically restructuring triangular grid.[4] A triangular grid avoids problems of mesh tangling encountered in Lagrangian implementations using a quadrilateral mesh. Individual mesh points are reconnected to allow for the migration of fluid elements in the flow field. Since the number of grid lines meeting at a vertex is variable, the resolution can be altered where needed (e.g., around the droplet in the combustion zone) without affecting the resolution in other areas of the computation. Integral equations are used to specify the values of physical variables during grid restructuring to ensure that the evaluation of the fluid flows are fully conservative.

In this presentation we describe calculations of inviscid, incompressible fluid flow about non-reacting droplets for a variety of flow speeds and droplet densities. The evolution of the flow field external and internal to the droplet will be shown. Preliminary results which include the effects of surface tension will also be shown. The algorithms for a particularly simple extension to compressible flows will be discussed for the case in which heat release occurs on a time scale fast compared to the fluid flow. When the time scales are comparable, or if the effects of shocks are important, other algorithms must be used, and alternate formulations will be presented.

Future work on this project will incorporate the compressibility algorithms into the code together with the effects of viscosity. Algorithms for calculating reactions, vaporization, thermal conduction and molecular diffusion will be taken from other reactive flow codes.[5] The addition of each of these processes into the code will be accompanied by benchmarking on pertinent physical problems. An r-z version of the code is being developed in parallel with the Cartesian version, and initial tests of this code using circular Couette flow and Taylor vortex flow will be presented as well.

Acknowledgment

This work is funded in part by the National Aeronautics and Space Administration and by the Office of Naval Research.

References

1. Williams, A., "Combustion of Droplets of Liquid Fuels: A Review," Combustion and Flame 21, 1 (1973).

2. Faeth, G.M., "Current Status of Droplet and Liquid Combustion," Prog. Energy Combust. Sci. 3, 191 (1977), and Faeth, G.M., "Evaporation and Combustion of Sprays," Prog. Energy Combust. Sci., to be published.

3. Fritts, M.J., E.S. Oran and J.P. Boris, "Lagrangian Fluid Dynamics for Combustion Modelling," NRL Memorandum 4579, 1981.

4. Fritts, M.J. and J.P. Boris, "The Lagrangian Solution of Transient Problems in Hydrodynamics Using a Triangular Grid," J. Comp. Phys. 31, 173 (1979).

5. Oran, E.S., and J.P. Boris, "Detailed Modelling of Combustion System," Prog. Energy Combust. Sci. 7, 1 (1981) and Oran, E.S., J.P. Boris, T. Young, M. Flanigan, T. Burks and M. Picone, "Numerical Simulations of Detonations in Hydrogen-Air and Methane-Air Mixtures," Eighteenth Symposium (International) and Combustion p. 1641, The Combustion Institute, 1981.

The results were also reported on at the American Physical Society, Division of Fluid Mechanics Meeting in Monterey, CA in November 1981. An abstract follows:

Numerical Calculations of Flow in and around a Droplet, D.E. Fyfe*, M.J. Fritts, and E.S. Oran, Naval Research Laboratory. Complicated flow fields arise in and around burning fuel droplets. Here we present the initial results of numerical simulations aimed at providing a description of these flows. These initial calculations show the results of inviscid incompressible fluid flow in and about a non-reacting fuel

*Science Applications, Inc., McLean, VA 22102
This work is funded in part by the NASA and in part by the ONR.

droplet. The simulations were performed using a Lagrangian algorithm with a dynamically restructuring triangular grid. These algorithms allow variable sized cells, addition and deletion of cells, and continuous calculation without diffusive rezoning. We present the evolution of the flow fields for several flow speeds and droplet densities. Preliminary results incorporating the effects of surface tension will also be shown. More realistic calculations in the future will have to include viscosity, thermal effects, vaporization, molecular diffusion, chemical reactions and compressibility. Algorithms for the extension to compressible flows when heat release occurs on a time scale fast compared to the fluid flow will be discussed.

REFERENCES

1. Fluid Dynamics-Reactive Flow Modeling, Final Report #SAI-82-655-WA. See Appendix B. This report will appear in Combustion and Flame, 1982.

2. Dabora, E.K.: Effect of Additives on the Lean Detonation Limit of Kerosene Sprays. UCONN0507-129-F, The University of Connecticut, 1980.

3. Lee, J.H., Knystantas, R. and Guirao, C.M.: Fifteenth Symposium (International) on Combustion, p. 53, the Combustion Institute, 1975.

FIGURE CAPTIONS

Figure 1 Calculation of droplet deformation in an external flow.

Figure 2 Vertex pathlines showing fluid flow inside and outside deforming droplet.

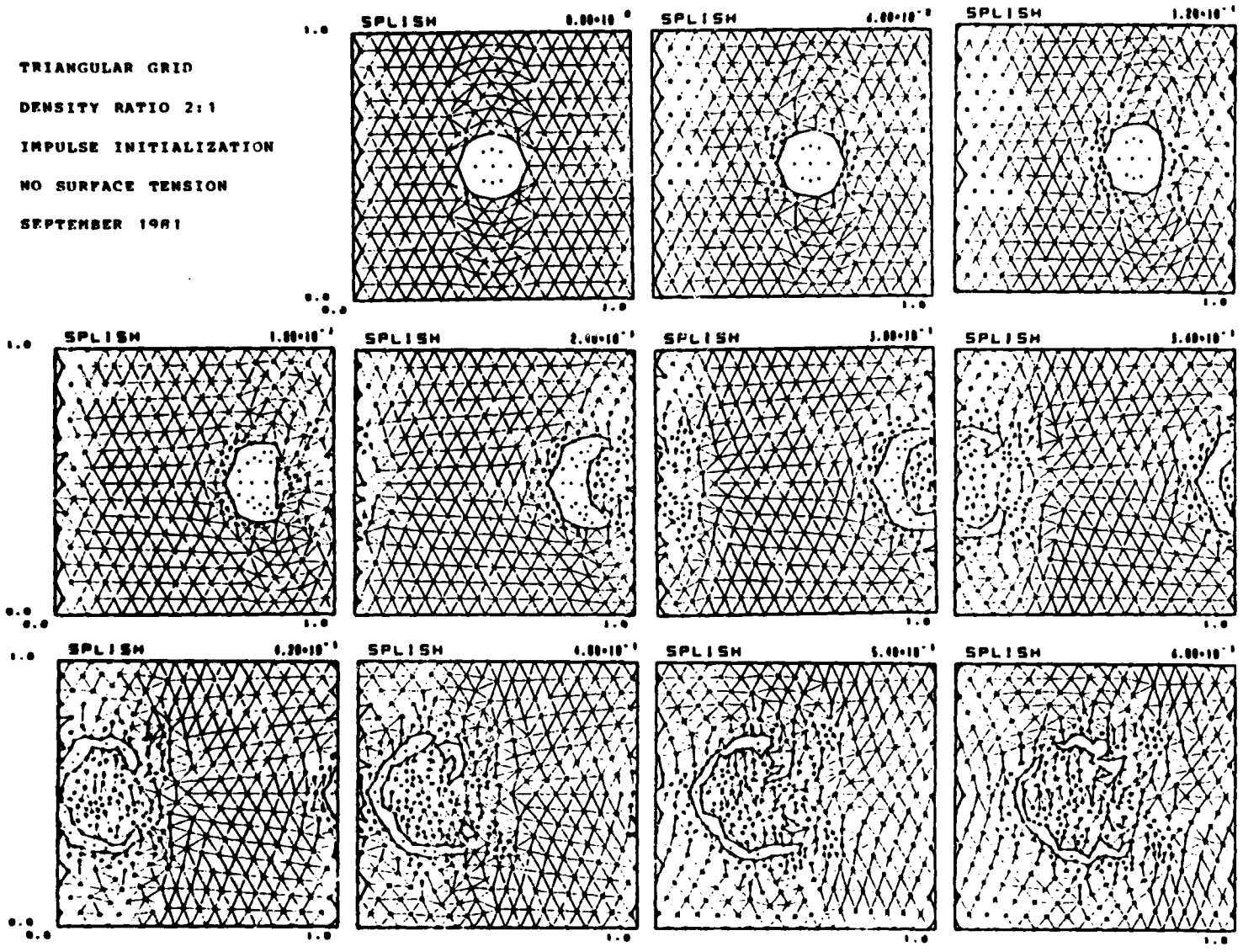
TRIANGULAR GRID
DENSITY RATIO 2:1
IMPULSE INITIALIZATION
NO SURFACE TENSION
SEPTEMBER 1981
SPLISH
SPLISH
SPLISH
SPLISH
SPLISH
SPLISH
SPLISH
SPLISH
SPLISH
SPLISH
SPLISH
SPLISH

Figure 1

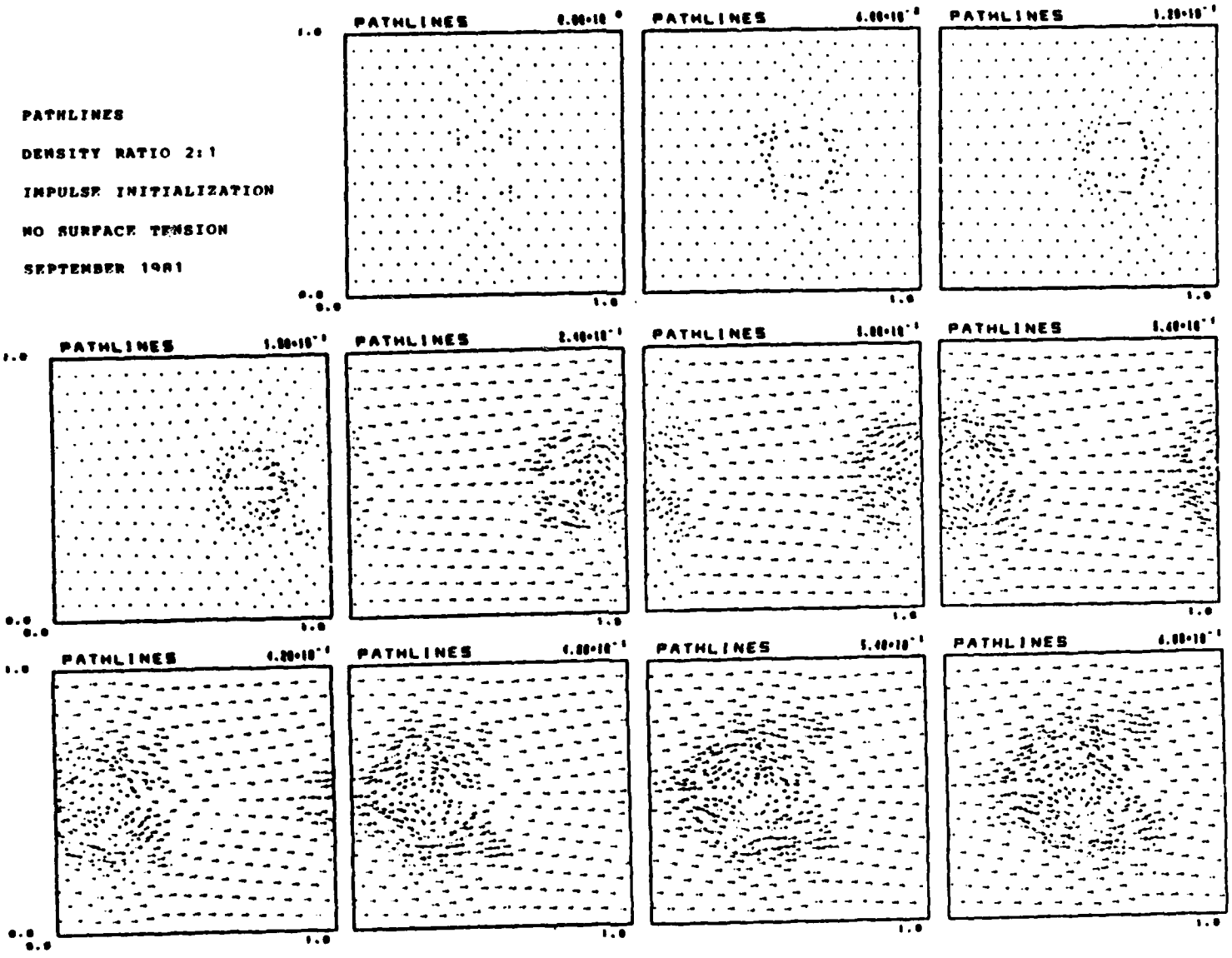
PATHLINES
DENSITY RATIO 2:1
IMPULSE INITIALIZATION
NO SURFACE TENSION
SEPTEMBER 1981
PATHLINES
PATHLINES
PATHLINES
PATHLINES
PATHLINES
PATHLINES
PATHLINES
PATHLINES
PATHLINES
PATHLINES
PATHLINES
PATHLINES

Figure 2

Appendix A

TIME-DEPENDENT SIMULATION OF FLAMES IN HYDROGEN-OXYGEN-NITROGEN MIXTURES

Time-Dependent Simulation of Flames in Hydrogen-Oxygen-Nitrogen Mixtures

K. Kailasanath*, E.S. Oran, J.P. Boris, and T.R. Young
Laboratory for Computational Physics
Naval Research Laboratory
Washington, D.C., 20375

1. INTRODUCTION

This paper describes a one-dimensional, time-dependent, Lagrangian model developed to study the initiation, propagation and quenching of laminar flames. The model incorporates a number of new approaches and algorithms which have now been tested by comparisons to less complex or analytic solutions and by comparisons to experimental data. These new elements include: ADINC [1] an implicit, Lagrangian method for solving the convective parts of the conservation equations; DFLUX [2,3] a variable accuracy algorithm for determining diffusion fluxes without having to invert matrices; SPLIT and MERGE, routines for dividing or merging computational cells as specified by external criteria; VSAIM, a vectorized version of the ordinary differential equation solver, CHEMEQ [4,5]; and a new method for treating an open boundary in an implicit, Lagrangian calculation. An asymptotic coupling method, used in conjunction with timestep splitting to couple the various processes, allows the use of entirely different algorithms for the physical processes represented by different mathematical forms.

The model has been used for a variety of flame studies of hydrogen-oxygen-nitrogen mixtures. These include calculations of minimum ignition energies, flammability limits, quench volumes, and burning velocities. The chemical rate scheme has now been tested extensively, as have the thermal and molecular diffusion coefficients. Thus we expect the model to calculate correctly the time-dependent behavior implied by the initial and boundary conditions supplied.

*Currently with Science Application, Inc. McLean, VA

After a summary is given of the important numerical features, several calculations are presented. The first is a flame initiation and minimum ignition energy study of a mixture of $H_2:O_2:N_2/2:1:10$ initially at 298 K and 1 atm. These are inherently time-dependent problems and take advantage of this property of the model. The second problem discussed is a calculation of the burning velocity of the mixture $H_2:O_2:N_2/2:1:4$, again at 298 K and 1 atm. The burning velocity is a quantity used to describe a steady state property and it is generally calculated by steady state methods. We show below that the model described also does well on this type of calculation.

2. NUMERICAL MODEL

2.1 Basic Equations

We solve the time-dependent equations for conservation of total mass density ρ, momentum $\rho\underline{v}$, and energy E as well as the individual species number densities $\{n_j\}$. These may be written as [2,6]:

$$\frac{\partial \rho}{\partial t} = -\underline{\nabla}\cdot \rho\underline{v} \tag{1}$$

$$\frac{\partial n_j}{\partial t} = -\underline{\nabla}\cdot n_j\underline{V}_j - \underline{\nabla}\cdot n_j\underline{v} + P_j - L_j n_j \tag{2}$$

$$\frac{\partial \rho\underline{v}}{\partial t} = -\underline{\nabla}\cdot(\rho\underline{v}\underline{v}) - \underline{\nabla} P + \underline{\nabla}\cdot \eta_m[\underline{\nabla v} + (\underline{\nabla v})^T] \tag{3}$$

$$\frac{\partial E}{\partial t} = -\underline{\nabla}\cdot E\underline{v} - \underline{\nabla}\cdot P\underline{v} - \underline{\nabla}\cdot\underline{Q} \tag{4}$$

where the heat flux vector, $\underline{Q}$, is defined as

$$\underline{Q} = -\lambda_m \underline{\nabla} T + \sum_j n_j h_j \underline{V}_j + k_B T \sum_{j,k} \frac{n_j D_j^T}{N M_j D_{jk}} (\underline{V}_j - \underline{V}_k) \tag{5}$$

The quantity $\underline{v}$ is the fluid velocity, the $\{\underline{V}_j\}$ are the diffusion velocities, and $\{P_j\}$ and $\{L_j\}$ refer to the chemical production and loss processes for the individual species j. The quanties η_m and λ_m are the mixture viscosities and

thermal conductivities respectively. The superscript "T" in the last term of Eq. (3) indicates that the transpose is taken. The quantities $\{h_j\}$ are the temperature dependent enthalpies for each species, and the $\{D_{jk}\}$ and $\{D^T_j\}$ are the sets of binary and thermal diffusion coefficients, respectively.

We also assume that the mixture consists of ideal gases so that the pressure, P, may be written as:

$$P = Nk_BT \tag{6}$$

where N is the total number density, k_B is Boltzmann's constant and T is the temperature. The model presented in this report, however, is not restricted to ideal gases and in fact any equation of state may be used.

The diffusion equations may be written as

$$S_j = \sum_k \frac{n_j n_k}{N^2 D_{jk}} (\underline{V}_k - \underline{V}_j) \tag{7}$$

where the source terms S_j are defined as

$$S_j \equiv \underline{\nabla}\left(\frac{n_j}{N}\right) - \left(\frac{\rho_j}{\rho} - \frac{n_j}{N}\right) \frac{\nabla P}{P} - \sum_k \frac{n_j n_k}{N^2 D_{jk}} \left(\frac{D^T_k}{\rho_k} - \frac{D^T_j}{\rho_j}\right) \frac{\nabla T}{T} \tag{8}$$

The diffusion velocities are also subject to the constraint:

$$\sum_j \rho_j V_j = 0 \tag{9}$$

2.2 Convective Transport

The convective transport terms in Eqs. (1-4) are solved by the algorithm ADINC [1] . ADINC, designed for either Adiabatic or incompressible flows, is an implicit and Lagrangian algorithm. Since it communicates compression and expansion across the system implicitly, it overcomes the Courant time-step limit. Since it is Lagrangian, it can maintain steep gradients computationally for a long period of time. This is important in flame calculations where the diffusive transport of material and energy can govern the system evolution and therefore must be calculated accurately.

ADINC solves the following equations for mass and momentum transport in one dimension:

$$\frac{d\rho}{dt} = -\rho\, \underline{\nabla}.\underline{v} \tag{10}$$

$$\rho \frac{d\underline{v}}{dt} = - \underline{\nabla} P \qquad (11)$$

The energy evolution equation is eliminated by using an adiabatic equation of state:

$$\rho(P,S) = \rho_c + (P/S)^{1/\gamma} \qquad (12)$$

This equation of state with $\rho_c = 0$ is correct for adiabatic compression and expansion of an ideal gas. The entropy, S, is assumed constant throughout the numerical integration. Non-adiabatic processes, such as external heating, thermal conduction and chemical energy release, are added to Eqs. (10-11) using the timestep splitting methods described below.

Given an aproximation to the pressure, ADINC calculates the fluid density using Eq. (12). This equation-of-state density is compared to the density derived from the fluid dynamics through Eq. (10). The difference is iterated to zero using a quadratically convergent implicit solution of Eq. (11) which then gives an improved approximation to the pressure. During this iteration that analytic derivative $d\Lambda/dP$ is used where Λ is the volume of a computational cell. Thus

$$\frac{1}{\Lambda} \frac{d\Lambda}{dP} = - \frac{1}{\gamma \rho P} (P/S)^{1/\gamma} \qquad (13)$$

for the particular equation of state (12). ADINC also assumes that pressure and density are constant within each individual finite-difference cell and that the physics is evolving slowly enough for full communication across that cell to have occurred in a timestep.

ADINC has been used extensively for solving a wide variety of problems. Some of these and a number of tests of the algorithm have been documented by Boris [1].

2.3 Chemical Kinetics Calculations

The coupled, nonlinear, ordinary differential equations which describe the chemical interactions are taken from that part of Eq. (2), which represents the production and loss of reacting species:

$$\frac{\partial n_j}{\partial t} = P_j - L_j n_j \ , \ j = 1, \ . \ . \ . \ M, \qquad (14)$$

where M is the total number of species present. The functional dependencies of the terms

$$P_j = P_j\{n_k(t)\}$$

$$L_j = L_j\{n_k(t)\} \quad , k = 1, \ldots, M \tag{15}$$

emphasize the strong coupling between the various species. The system represented by Eq. (14) may be stiff when there are large differences in the time constants associated with different chemical reations. Stiffness may occur for different species, in different locations, at different times or simultaneously throughout the course of an integration. Because of this, when there are a large number of reactions, the solution of the chemical kinetics equations is usually the most expensive part of a detailed reactive flow calculation. Furthermore, the computational cost increases with the number of species and the dimensionality of the problem. Therefore a method which is efficient, accurate, conservative, stable and which does not require storage of large quantities of data from one timestep to another is required. Such a method is VSAIM, which is a fully vectorized version of the selected asymptotic integration method employed in CHEMEQ [4,5]. In this method, the stiff equations are identified and solved using a very stable asymptotic method. The remaining equations are solved using a standard classical method.

Once the species number densities are known, the temperature can be evaluated by iterating on the equation:

$$E_T - \frac{1}{2}\rho v^2 = \sum_j h_{o_j} n_j + \sum_j h_j n_j - P \tag{16}$$

where E_T is the total energy per unit volume, h_{o_j} is the set of heats of formation of the species j and h_j is the sensible enthalpy of species j. A Newton-Raphson iteration technique is used and it usually converges in two or three iterations per timestep.

2.4 Diffusive Transport

The diffusive transport processes considered in this model are molecular diffusion and thermal conduction. These are the parts of Eqs. (1-4) which are represented by the expressions:

$$\frac{\partial n_j}{\partial t} = - \underline{\nabla} \cdot n_j \underline{V}_j \tag{17}$$

$$\frac{\partial E}{\partial t} = \underline{\nabla} \cdot [-\lambda \underline{\nabla} T + \sum_j h_j n_j \underline{V}_j]. \tag{18}$$

The above equations are conservatively differenced and solved explicitly. The effects of viscosity and thermal diffusion have not been considered for the results discussed in this paper.

The diffusion velocities $\{V_j\}$ in Eqs. (17, 18) are determined by solving the equations [1,2]

$$S_j = \sum_{\substack{k=1 \\ k \neq j}}^{M} \frac{n_j n_k}{N^2 D_{jk}} (\underline{V}_k - \underline{V}_j) = \underline{\nabla} (n_j/N) - (\rho_j/\rho - n/N) \frac{\underline{\nabla} P}{P} \tag{19}$$

subject to the constraints

$$\sum_{j=1}^{M} S_j = 0, \text{ and } \sum_{j=1}^{M} \rho_j V_j = 0. \tag{20}$$

An iterative algorithm for solving for the diffusion velocities which avoids the cost of performing matrix inversions has been developed [2,3]. This algorithm DFLUX, is of $O(M^2)$ and is vectorized. Thus it is substantially faster than $O(M^3)$ matrix inversions when four or more species are involved.

Equations for the evaluation of diffusive transport coefficients have been discussed in detail by Picone [7] and summarized in Oran and Boris [2]. The forms given are for mixtures of neutral gases. Their derivations are based on or are advancements of the fundamental work of Chapman and Cowling [8] and Hirschfelder, Curtis and Bird [9]. Representations of the coefficients which are easily used in reactive flow models and not requiring the expensive inversion of matrices are chosen.

2.5 Timestep Splitting

In the asymptotic timestep split approach [2], the individual terms in the Eqs. (1-4) are solved independently as described above and then asymptotically coupled together. Since both chemistry and sound waves are usually stiff in deflagration problems, special care is required in coupling the chemical heat release to the fluid dynamics. In a flame, fluid dynamic expansion and diffusive transport relieve the pressure from the flame region as fast as it is generated. Thus the pressure stays effectively constant. Small pressure fluctuations, $O(v^2/c^2)$, do exist and are just large enough to drive the flows which reapportion the energy released by chemistry or transported by diffusion. The chemistry step should be taken at constant pressure, but it may also be taken at constant volume with temperature held fixed if the profiles only change slowly per timestep. At the completion of the chemistry integration, the heat release is converted to an effective pressure change at constant volume because the cell volume has been held fixed during the chemical kinetics calculation. This pressure change is then used as an energy source term for the fluid dynamics timestep to get the correct fluid expansion. This is done by modifying the cell entropies used as the fluid dynamics module, ADINC, described earlier. At this point thermal conduction and diffusion heat fluxes also contribute changes to the entropy.

2.6 Open Boundary Condition

In the study of unconfined flames, a representation for the open-boundary is required since the size of the computational domain is limited. One approach is to allow the computational cells to increase in size as they get further from the flame. Thus the computational domain is very large and there is no corresponding increase in computer storage. However, the cell stretching should be gradual to limit inaccuracies which arise as a result of the varying cell size.

A different approach used in the study of the propagation of unconfined flames is discussed below. Here the effects of an open boundary are accounted for by allowing the pressure

changes which occur in each cell during the timestep to relax adiabatically to the pressure before the time step. Due to this relaxation, the volume of the cell changes since a Lagrangian coordinate system has been used. The changes in the volume of the cells causes the location of the open boundary to change. The location of the open boundary and the fluid velocity in the last cell (which is also the velocity of the open boundary) are used as open boundary conditions. This procedure is appropriate because in unconfined flames the pressure stays effectively constant.

3. FLAMES IN HYDROGEN-OXYGEN-NITROGEN MIXTURES

Simulations of flames in hydrogen-oxygen-nitrogen mixtures have been carried out using the numerical model described above. Applying the model to a specific gas mixture requires knowledge of the chemical kinetic rate scheme and other species dependent input parameters such as thermal conducitvity and molecular diffusion coefficients.

The chemical kinetics rate scheme used consists of about fifty chemical rates relating the species H_2, O_2, H, O, OH, H_2O, HO_2 and H_2O_2. It has been extensively tested against experimental data [10, 11] and shown to give good results. Burks and Oran [10] showed that the results computed with the scheme compared very well with experimentally observed induction times, second explosion limits and the temporal behavior of reactive species. Oran et al. [11] have shown that the scheme gives good results when coupled with a fluid dynamic model in the simulation of the conditions behind a reflected shock. The reaction rate scheme has not been presented here since it is readily available [10,11,12]. Heats of formation and enthalpies have been taken from the JANAF tables [13].

The diffusion coefficients have been obtained using the data given by Marrero and Mason [14]. The Lennard-Jones (12:6) potential parameters σ and (ε/k) are those given by Svehla [15] except for σ_H and σ_{H2O} for which the values given by Dixon-Lewis [16] have been used.

Below we first discuss some of the results obtained in a study of the ignition and quenching of a $2:1:10/H_2:O_2:N_2$

mixture. Then we present results from a simulation of a propagating flame in a H_2-air mixture. In both cases, the initial temperatures and pressures of the unburned gas were 298 K and 1 atm, respectively.

3.1 Minimum Ignition Energies and Quenching Distances

The model described above is ideally suited for studying time-dependent problems such as the ignition of gas mixtures [12]. The model was configured in spherical geometry with an open boundary at one end to simulate a very large system. Energy was deposited in the center with a radius of deposition, R_o. Results from a typical calculation are presented in Fig. 1. The figure depicts the time history of the temperature profile after 4 mJ of energy is deposited over a period of 0.1 ms. Even after the energy deposition is stopped, the central temperature continues to increase due to the heat released in chemical reactions. With time, however, the temperature near the center decreases and the temperature away from the center increases due to diffusive transport. By 4.5 ms, we see that the temperature distribution exhibits a "flame" temperature profile. If the amount of energy deposited, E_o, was reduced to 3 mJ, the temperature distribution does not develop into a flame temperature profile.

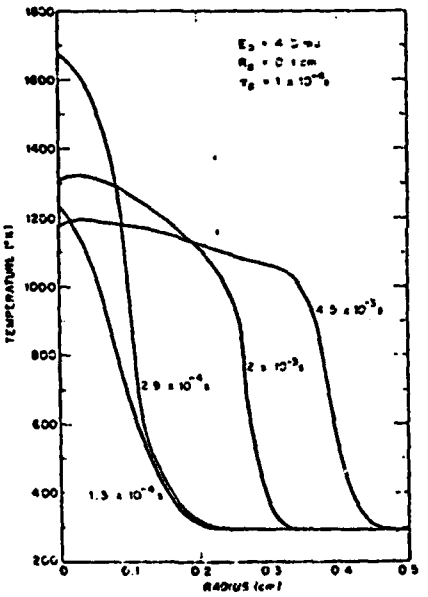

Fig.1. Time history of the temperature profile.

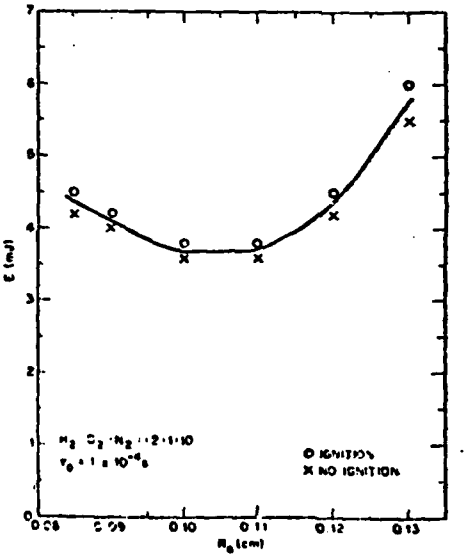

Fig.2. Minimum ignition energy as a function of radius of energy deposition.

By repeating the computations for different values of E_o, a bound for the minimum ignition energy for that particular radius was obtained. Similar calculations were performed for different values of the radius of deposition, R_o. The results of such investigations are shown in Fig 2. A propagating flame results when 3.8 mJ of energy is deposited in a sphere with a radius of 0.1 cm. However if the same amount of energy is deposited in a sphere of smaller radius, the rate of heat liberation is insufficient to compensate for the rate of heat loss and consequently there is no ignition. This radius, 0.1 cm, is the "quench-radius" for this particular mixture. For radii slightly larger than the quench-radius, the minimum ignition energy is almost constant and for larger radii (larger than 0.11 cm) the minimum ignition energy increases rapidly with increasing radii. Therefore for the system under study, the absolute minimum energy is about 3.7 mJ. These observations are in qualitative agreement with those of Lewis and von Elbe [17]. Quantitative comparisons are not possible since the composition of the mixture and the time for energy deposition are different.

3.2 Calculation of the Burning Velocity of an $H_2:O_2:N_2/2:1:4$ Mixture at 298K. 1 atm.

The model described above can also be used to study the propagation of flames in pre-mixed gas mixtures. As shown in Fig. 1, if sufficient energy is deposited at the center of a sphere and computations are carried out for a sufficiently long time, the temperature distribution attains a typical "flame profile". However, this method is an expensive way to generate a propagating flame since so much time is spent in establishing and overcoming the initial conditions. Another method for initializing the problem quickly is to start the computations with a good guess for the temperature and species profile in a region behind a flame front. The closer the initial profiles are to the final, steady state flame profile, the sooner the initial conditions relax to the steady propagating flame. This procedure was adopted for obtaining the values for a flame velocity.

The model was set up in cartesian geometry with one end closed (preventing any gas flow through it) and the other open to the atmosphere. At the closed end, a first approximation to the temperature and major species profile was set up as initial conditions. This soon evolves into a propagating flame as can be seen in Fig. 3, where the temperature profiles at 50 μs and 60 μs (from the start of the computations) are shown. However, in order to determine the flame speed, a criterion for the location of the flame is required. An arbitrary value of 900K is chosen to define the location of the flame. The movement of the location of this value (900K) in time and space gives the rate of propagation of the flame. The location of the flame is presented as a function of time in curve (a) in Fig. 4. The slope of this curve gives the flame velocity (for an inertial observer). From this figure we see that the flame propagates initially at a velocity of 8.7 m/s and by 50 μs (from the start of the computations) it attains a nearly constant value of 9.7 m/s.

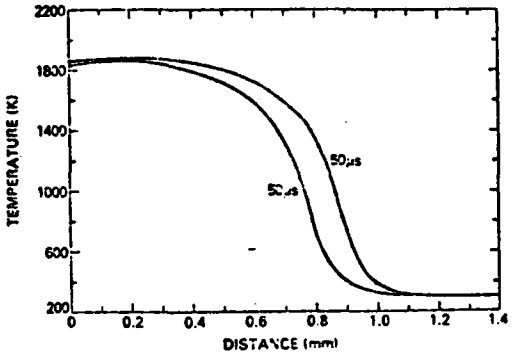

Fig.3. Temperature profiles in a propagating flame.

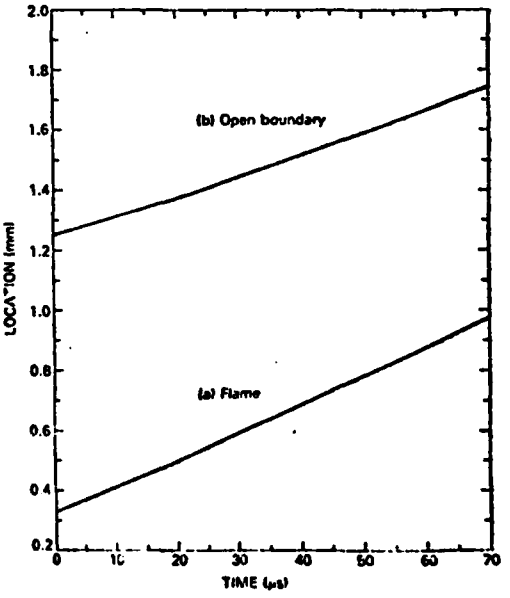

Fig.4. Time history of the location of (a) the flame and (b) the open boundary.

A quantity of considerable practical interest is the burning velocity which is defined as the rate at which the

flame consumes the reactants, or equally well as the flame velocity relative to the unburned gases. In Fig. 5 the fluid velocity profile in the system is depicted at a particular time. The velocity is zero at one end since that end is a closed boundary. The flow velocity increases across the flame and is maximum at the open boundary. An estimate for the burning velocity can be obtained by subtracting the velocity of the unburned gases from the flame velocity. An upper estimate for the velocity of the unburned gases is the fluid velocity at the open boundary. Since this model uses a Lagrangian coordinate system, the fluid velocity at the open boundary is also given by the rate of movement of the open boundary. The location of the open boundary has been depicted as a function of time in Fig. 4 b . Corresponding to a flame velocity of 9.7 m/s we see that the velocity of the unburned gases (open-boundary) is about 7.6 m/s giving a burning velocity of 2.1 m/s for the hydrogen-air flame studied. This compares well with the experimental values for the burning velocity [18] which are between 2 and 2.5 m/s.

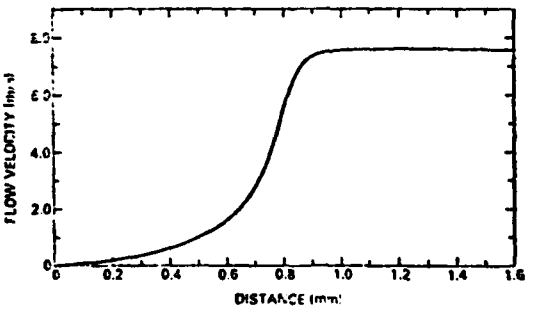

Fig.5. Flow velocity profile in a propagating flame.

IV. CONCLUSIONS

In this paper we have shown that the time-dependent model described does a good job in predicting both transient and

steady state properties of laminar hydrogen-oxygen-nitrogen flames. In the calculations of the burning velocity of a mixture of $H_2:O_2:N_2/2:1:4$ at 1 atm and 298 K, the velocity predicted was at the lower end of the observed range. We note, however, that there are several factors which would tend to increase this estimated value. First, the calculated burning velocity would be larger if the velocity of the unburned gas used in this calculation were closer to the flame front instead of at the open boundary. It is not clear where it should be evaluated. Second, if thermal diffusion is included, it would increase the flame velocity by perhaps 5-10%. Finally, the extremely important hydrogen diffusion coefficients are not really known at high temperatures. If they are higher than the ones used here, the flame velocity would increase. These observations lead us to believe that the higher observed values of the burning velocity are probably more accurate.

Finally, we wish to note that the method is sensitive to initial conditions. As in the steady-state calculations, a better initial guess leads to faster convergence to a steady propagating flame. Perhaps the best way to initialize such a problem is to perform a two step process in which we first determine the minimum ignition energy for a given radius and time of energy deposition, and then deposit this energy and evaluate the properties of the propagating flamefront. However, considering that the experimental velocities vary by ~25%, a good initial guess at temperature and species concentrations certainly gives an adequate calculation. Finally, we note that the criterion on which to judge the initial guess values is to look at how flat the temperature profile is behind the flamefront. A bad guess produces some structure and oscillations which only slowly disappear.

ACKNOWLEDGEMENTS

We wish to thank Dr.J.M. Picone for many useful conversations and insights. This work was sponsored by the Office of Naval Research through the Naval Research Laboratory and by the Naval Material Command.

REFERENCES

1. Boris, J.P., ADINC: An Implicit Lagrangian Hydrodynamics Code, N.R.L. Memorandum Report 4022, Naval Research Laboratory, Washington, D.C. , 1979.

2. Oran, E.S., and Boris, J.P., Prog. Energy Combustion Science. 7:1-72 (1981).

3. Jones, W.W., and Boris, J.P., Comp. Chem. 5, 139-146 (1981).

4. Young, T.R., and Boris, J.P., J. Phys. Chem. 81, 2424-2427 (1977).

5. Young, T.R., CHEMEQ, A Subroutine for Solving Stiff Ordinary Differential Equations, N.R.L. Memorandum Report 4091, Naval Research Laboratory, Washington, D.C., 1980.

6. Williams, F.A., Combustion Theory, Addison Wesley, Reading, MA., 1965, p.2.

7. Picone, J.M., and Oran , E.S., Approximate Equations for Transport Coefficients of Multi-component Mixtures of Neutral Gases, N.R.L. Memorandum Report 4384, Naval Research Laboratory, Washington, D.C., 1980.

8. Chapman, S., and Cowling, T.G., The Mathematical Theory of Non-uniform Gases, Cambridge University Press, 1970.

9. Hirschfelder,J.O., Curtiss, C.F., and Bird, R. B., Molecular Theory of Gases and Liquids, John Wiley and Sons, Inc., New York, 1954.

10. Burks, T.L., and Oran, E.S., A Computational Study of the Chemical Kinetics of Hydrogen Combustion, N.R.L. Memorandum Report 4446, Naval Research Laboratory, Washington, D.C., 1980

11. Oran, E.S., Young, T.R., Boris, J.P., and Cohen, A., Weak and Strong Ignition-I, N.R.L. Memorandum Report 4664, Naval Research Laboratory, Washington, D.C., 1981. (Also to appear in Combust. Flame).

12. Kailasanath, K., Oran, E.S., and Boris, J.P., A Theoretical Study of the Ignition of Pre-Mixed Gases, 1982 (to appear in Combust. Flame.)

13. Stull, D.R., and Prophet, H., JANAF Thermochemical Tables, National Standard Reference Data Series, U.S. National Bureau of Standards, No. 37, 2nd Ed., Gaithersburg, Maryland, 1971.
14. Marrero, T.R., and Mason, E.A., J. Phys. Chem. Ref. Data, 1,3-118 (1972).
15. Svehla, R.A., Estimated Viscosities and Thermal Conductivities of Gases at High Temperatures, Technical Report No. R-132, NASA, Washington, D.C., 1962.
16. Dixon-Lewis, G., Combust. Flame, 36, 1-14 (1979).
17. Lewis, B., and von Elbe, G., Combustion, Flames and Explosions of Gases, Academic Press, New York, 1961, p. 326.
18. Warnatz, J. Ber. Bunsenges. Phys. Chem. 82, 643-649 (1978).

Appendix B

DIRECT INITIATION OF GASEOUS DETONATIONS IN SHOCK TUBES: NUMERICAL SIMULATIONS OF EXPERIMENTS

DIRECT INITIATION OF GASEOUS DETONATIONS IN SHOCK TUBES: NUMERICAL SIMULATIONS OF EXPERIMENTS

by:

K. Kailasanath*, E. S. Oran, T. R. Young and J. P. Boris
Laboratory for Computational Physics
Naval Research Laboratory
Washington, D.C. 20375

and

E. K. Dabora
Department of Mechanical Engineering
The University of Connecticut
Storrs, Connecticut 06268

Subject Heading:

(22) Supersonic Flow with Reaction

(23) Theory of Deflagration and Detonation

(33) Detonation Dynamics

Address Correspondence to:

Dr. K. Kailasanath
c/o Code 4040
Naval Research Laboratory
Washington, D.C. 20375

---

*Currently with Science Applications, Inc., McLean, VA

ABSTRACT

Detailed numerical simulations of shock tube experiments have been used to study the direct initiation of detonations in hydrogen-air mixtures. Whereas these simulations qualitatively agree with earlier experimental observations that a minimum power, a minimum energy and some relation between them is required to characterize the direct initiation of detonations, the experiments and calculations do not agree well quantitatively. During the course of this study it was found that the disagreement is primarily because the induction times of the gaseous mixtures, at the temperatures and pressures expected behind the incident shocks, are very sensitive to perturbations in pressure and temperature. Simulations carried out to evaluate the effects of sound wave perturbations on one of the gas mixtures studied give a quantitative relation between the induction time and sound wave perturbations in a range of amplitudes and frequencies. It is shown that the presence of such perturbations can produce experimentally determined minimum powers and minimum energies which are significantly different from those calculated.

I. INTRODUCTION

The widespread use of natural gas, methane and other gaseous fuels has made it increasingly important to understand and quantify their tendency to detonate. The early works[1,2,3] on the initiation of detonations established the importance of the magnitude of the source energy in the direct initiation of gaseous detonations. More recent experiments[4,5,6] have shown that not only is the amount of energy important but also the rate at which the energy is deposited, namely, the power. The experimental results of Lee et al.[5] indicate that there is a critical detonation energy below which a detonation would not occur no matter what the power is and that there is a critical power below which a detonation would not occur no matter what the total energy is. The requirement for a critical value for the power of the source indicates that the source must be capable of generating a shock wave of certain minimum strength. The critical energy requirement implies that the shock wave must be maintained at or above this minimum strength for a certain duration.

Recently these ideas have been used to obtain a relation between the power and energy requirement for direct initiation of detonations in a shock tube.[7] In a shock tube, for a given set of driver and driven gases, the pressure ratio across the diaphragm determines the strength

(Mach Number) of the shock wave generated. Therefore, by varying the pressure ratio across the diaphragm, the power of the source can be varied since it depends on the shock strength. When the diaphragm is burst, rarefaction waves are generated in the driver section of the shock tube. If a short driver section is used the rarefaction waves can reach the shock front after reflection from the driver end wall and reduce the shock velocity. If the wave is a detonation, it is expected that the wave will continue to propagate unhampered by the rarefaction waves. For a specific driver length, we can determine the pressure ratio (and hence the minimum power) below which the rarefaction waves will interact with the shock wave and cause it to decay before ignition can occur. The corresponding minimum detonation energy can be obtained if the time for which the shock wave is effective is known. By repeating the experiments with different driver lengths, we can determine different sets of minimum power and minimum energy required to initate detonations. Then, from a plot of these minimum powers as a function of the minimum energies, one can determine the critical power (the lowest value of the minimum power) and the critical detonation energy (the lowest value of the minimum energy).

In the shock tube experiments,[7] the initiation of stoichiometric hydrogen-air mixtures with drivers of three different lengths was investigated. For each driver, the

location at which the Chapman-Jouguet Mach Number was reached was noted for various pressure ratios. From this the pressure ratio below which detonation was expected to take place at extremely long distances from the diaphragm was estimated. Using this information and a simple theoretical model a relation between the minimum detonation energy and the minimum power was also obtained.

In this paper, we have used numerical simulations to examine several aspects of the basic idea of using shock tube experiments to study the direct initiation of detonations. First, we establish the importance of the power in the direct initiation of detonations. Then we show that the results from the numerical simulations are very different from the experimental results. The reasons for the discrepancy are examined and discussed in detail. First, the experiments are shown to be in a pressure-temperature regime which is very sensitive to perturbations[8,9] and second, the experiments were very susceptible to such perturbations because the driver and driven sections had different areas of cross-section and were of different shapes. Finally, we examine this sensitivity of the ignition process in the hydrogen-air mixture by using numerical simulations to evaluate the effect of sound wave perturbations on ignition.

II. THE NUMERICAL MODEL

The one-dimensional NRL Reactive Shock Model[10,11] used to perform the calculations described below solves the time-dependent conservation equations[11,12] for mass, momentum and energy coupled to the equations describing the chemical kinetics. Though the geometry may be either cartesian, cylindrical, spherical or some generalized coordinate, here we consider cartesian geometry. The model uses an explicit, Eulerian finite difference formulation with a sliding rezone capability to provide resolution around moving gradients.

The convective transport terms in the conservation equations are solved using one variant of the Flux-Corrected Transport (FCT) method.[13,14] This is a conservative, monotonic algorithm with fourth-order phase accuracy and does not require artificial viscosity to stabilize shocks. The Flux Correction procedure itself ensures that the shocks are one or two zones wide and have maximal resolution. The ordinary differential equations describing the chemical kinetics are solved using YSAIM, a vectorized version of the selected asymptotic integration method employed in CHEMEQ.[15,16] This algorithm identifies the stiff equations for treatment with a stiffly stable method. The remaining equations are solved with a standard classical method. The algorithm has been specially optimized for use in conjunction with fluid dynamic models.

For calculations performed in this paper the time-scales under consideration are short and therefore the diffusive transport processes, thermal conduction and molecular diffusion, have negligible effect. The calculations performed in this paper do not include these processes although they are part of the NRL Reactive Shock Model. The solutions for the equations describing the fluid dynamics and the chemistry of the problem are coupled using time-step splitting techniques.[11]

The chemical kinetics rate scheme used consists of about fifty chemical rates relating the species H_2, O_2, H, O, OH, HO_2, H_2O and H_2O_2. It has been extensively tested against experimental data[8,17] and shown to give good results. Burks and Oran[17] showed that the results computed with the scheme compared very well with experimentally observed induction times, second explosion limits and the temporal behavior of reactive species. Oran et al.[8] have shown that the scheme gives good results when coupled with a fluid dynamic model in the simulation of the conditions behind a reflected shock. The reaction rate scheme has not been presented here since it is readily available.[8,17] Heats of formation and enthalpies have been taken from the JANAF tables.[18]

The detailed simulations of the shock tube experiments discussed in this paper require that we not only

model very long systems but that we also accurately model the movement of the contact surface and the reactive shock wave. A rather sophisticated adaptive gridding method has been developed for this purpose at NRL by Oran and Young.[19] There are two finely gridded regions: one surrounding and moving with the shock wave and the other surrounding and moving with the contact surface. Each of these finely gridded regions may have a different minimum computational cell size. The regions ahead of the shock wave and behind the contact surface have computational grids in which the cells change exponentially in size from the smallest surrounding the shock wave or the contact surface to the largest at the walls. Care is taken that the transition in the cell sizes is smooth. For the results presented in this paper a total of 165 computational cells are used to describe the shock tube and the cell sizes varied from 0.1 cm around the shock to over 50 cm near the shock tube end-walls.

III. NUMERICAL SIMULATIONS

The numerical model described in the preceeding section was first used to study a selected group of the shock tube experiments described briefly in the introduction and more completely by Dabora.[7] In the experiments, the driven section of the shock tube was 9 feet (≈2.75m) long with 2" x 2" square cross section. The driven section contained a hydrogen-air mixture at 0.5 atm (50.66 kPa). The driver section contained helium, was variable in length (2", 4" or 8") and had a circular cross section providing a driver to driven area ratio of 1.65.

The simulations described below are for a shock tube with a 20 cm (≈8") driver section filled with helium and a 280 cm driven section filled with a mixture of H_2-O_2-N_2/2-1-4 at 0.5 atm and 298 K. However, in contrast to the experimental set-up, the entire tube was assumed to be of uniform cross section.

One of the problems with numerical simulations is interpreting the large quantity of output data. At each time step we calculate mass, momentum, energy, temperature, and a number of species densities. In order to compare the simulations most effectively with the experiment, we have chosen to follow the time-dependent behavior of three quantities: the velocity of the shock or detonation, the velocity of the contact surface and the pressure behind

the leading edge of the shock or detonation wave. Typical values of these quantities are shown in Fig. 1 for a pressure ratio of 110 across the diaphragm. After the diaphragm is burst, the velocity of the contact surface (Fig. 1b) is almost constant until about 0.6 ms and then it decreases continuously because of interactions with the rarefaction waves reflected from the driver end-wall. When the front of the rarefaction waves finally catches up with the shock front, the shock velocity and pressure are reduced. The shock does not transition to detonation during the time (1.6 ms) for which the simulation was carried out.

Results from a simulation corresponding to a pressure ratio of 150 are depicted in Fig. 2. Here ignition was first observed at about 0.14 ms near the contact surface. The chemical energy released causes a rapid rise in the temperature and the pressure near the contact surface whose velocity then changes rapidly. The entire region between the contact surface and the shock front had ignited by 0.15 ms. The pressure behind the shock front increases greatly at about this time and then decreases towards a constant value. The shock transitions to a detonation around 0.15 ms. There are oscillations in the shock velocity during the transition period as well as for a short time after the diaphragm is burst. However, by about 0.2 ms the oscillations die down and the detonation

velocity gradually decreases towards the Chapman-Jouguet detonation velocity. During the time oscillations were observed, a least squares approximation was used to obtain a fit for the shock or detonation front velocity.

These calculations can be used to evaluate the power, which is the rate of energy input to the driven section. The power is equal to the rate of work performed by the contact surface which is the product of the pressure at the contact surface and the velocity of the contact surface. The pressure at the contact surface is directly obtained from the simulations while the velocity of the contact surface is calculated from the time history of the location of the contact surface.

The time history of the power and energy for the two cases discussed in detail above are shown in Fig. 5. In the case where the pressure ratio was 110, the power is nearly constant until about 0.6 ms and then it decreases as the pressure and the fluid velocity at the contact surface decrease. Figure 5a shows that the power decreases from about 0.9 GW/m^2 to about 0.34 GW/m^2 by 1.6 ms. The energy input to the driven gas increases linearly until 0.6 ms since the power is constant. It then increases less rapidly as the power decreases with time. We note that an energy of 1.12 MJ/m^2 is not sufficient to cause a detonation in this case. In the case where the pressure ratio

was 150 (Fig. 5b), the power is almost constant until 0.14 ms, rises rapidly and fluctuates until about 0.24 ms, and then remains constant until the end of the simulation. The rapid rise in the power is due to the interaction of the contact surface with pressure waves generated by combustion. The significance of the power after ignition occurs is not clear since then the energy released in chemical reactions interact with the motion of the contact surface. The energy input to the driven gases up to ignition is only 0.135 MJ/m^2.

In summary, we observe from these simulations that the 0.9 GW/m^2 initial power with an energy input of 1.12 MJ/m^2 does not initiate a detonation while the 1.1 GW/m^2 initial power corresponding to 0.135 MJ/m^2 energy input does. This indicates that both a minimum power, a minimum energy and some relation between them are required to characterize the initiation of detonations. However, before any further effort goes into determining them, it is important to validate this approach by comparing the calculated and experimental results.

The pressure ratios and the corresponding detonation locations observed in the experiments and in the simulations are shown in Fig. 4. Both the simulations and the experiments show that as the pressure ratio is decreased, detonation occurs further and further from the diaphragm. However, the numerically predicted pressure ratio below

which a detonation will occur far from the diaphragm as well as the locations of the detonations are very different from the experimental results. Part of the difference between the experimentally and numerically determined locations is due to different criteria used to determine them. The experimental locations are determined by the observation of a "steady," Chapman-Jouguet detonation velocity while the numerically determined locations are those at which an "unsteady" detonation wave is first observed. In the simulations, the detonation velocity was found to be gradually decreasing towards a steady value when the computations were terminated. Longer runs are required to determine the location at which the detonation wave becomes steady.

A possible explanation for the differences in the pressure ratio for which detonations are observed could be the difference in the driver to driven area ratio. For a specific pressure ratio, the higher area ratio in the experiments may result in a shock of higher Mach number compared to those simulated. However, the Mach numbers of the shocks actually observed in the experiments (Fig. 4) were all lower than those in the simulations. Therefore an alternate explanation is required for the discrepancy between the two results.

The disagreement between the predictions of the numerical model and the experimental results is similar to that observed in an earlier study of weak ignition systems by Oran and Boris.[8,9] They found that ignition in mixtures of hydrogen and oxygen in certain regimes of the pressure-temperature plane are extremely sensitive to sound wave and entropy wave perturbations. In the next section, the discrepancy in the results is examined on the basis of this observation.

IV. SENSITIVITY OF IGNITION TO PERTURBATIONS

The sensitivity of ignition to perturbations can be assessed by considering derivatives of the chemical induction time with respect to parameters of the system such as temperature, pressure, or stoichiometry. One important quantity to consider is

$$S = -(T/\tau)(\partial\tau/\partial T|_s),$$

which shows the sensitivity of the induction time, τ, to sound wave perturbations.[9] Here T and s are the initial temperature and entropy, respectively. It has been shown[9] that high values of S indicate large variations in the ignition time for small changes in pressure and temperature. The value of S for the conditions behind the incident shock in the calculations discussed above were all between 35 and 40, indicating a fairly strong susceptibility of ignition times to perturbations. This means that 2.5-3% change in temperatures changes the induction time by 100%.

In order to evaluate quantitatively how a specific type of perturbation affects ignition, we have simulated the effects of sound waves in H_2-O_2-N_2 mixtures by reconfiguring the numerical model described earlier. The particular case we will investigate here is that for the pressure ratio of 110, which corresponds to a high value of S in the calculations considered in the previous section. We consider a homogeneous mixture of H_2-O_2-N_2/2-1-4 at 975K and 800kPa.

At the beginning of these simulations, a velocity perturbation is imposed on the system at each location x such that

$$v(x,t=0) = v_o \sin(\frac{\pi}{L} x)$$

where v_o is the amplitude and L is the half wavelength of the sound wave perturbation. We determine L by deciding how many periods of the wave we wish to occur during a chemical induction time.

Figure 5 shows the time history of the temperature taken from one simulation in which there are roughly three periods of sound wave oscillation in an induction time. In this case, L is 90 cm (giving a frequency of 403 Hz) since the induction time is 7380μs. The amplitude of the perturbation, v_o, is 100m/s. With this perturbation, the system ignites first at the left wall at 4923μs, then at the center and finally at the right wall at 5091μs. Thus we observe that the time to ignition is reduced by 2457μs due to the sound wave perturbation.

Figure 6 summarizes the results of a number of calculations similar to the one presented in Fig. 5. Here we have plotted the time at which ignition is first observed as a function of v_o for a range of values of L. For example, if L is 90cm, perturbations with amplitudes greater than 100m/s reduce the induction time substantially. Considering the curves for two values of L, namely 45cm and 90cm, we note that for low amplitude perturbations (less than 250m/s), the

lower frequency perturbations cause ignition earlier than the higher frequency perturbation. The trend is reversed for higher amplitude perturbations (greater than 250m/s). This difference can be explained by considering the number of periods of oscillation that occur before ignition. For the higher amplitude perturbations, the detailed simulations show that ignition occurs during the first period of the perturbations. Since the period of oscillation is shorter with the high frequency perturbations, ignition occurs earlier in that case. For lower amplitude perturbations, the system undergoes more than one period of oscillation before ignition. Although the period itself is longer for lower frequency perturbations, the residence time for the reactive mixture in a perturbed state is also longer. Therefore, for low amplitude perturbations, when more than one period of oscillation occurs before ignition, the lower frequency perturbation causes earlier ignition. This competition between the residence time in a perturbed state and the period of oscillation explains the intersection of the curves in Fig. 6.

We also observe from Fig. 6 that low frequency perturbations are more critical, since for these frequencies smaller amplitude perturbations are sufficient to substantially reduce the ignition times. For example, to reduce the time for

ignition by a factor of three, we need low frequency perturbations (L = 270cm) of amplitude 100m/s or higher frequency perturbations (L = 2.7cm) of amplitude 330m/s. [We also note that in the limit of no frequency (i.e., local hot spots) a small temperature perturbation could have an enormous effect on the ignition time.]

In the previous section, we noted differences between the experimental results and the numerical predictions of the initiation of detonations. Specifically, for a pressure ratio of 110, the numerical predictions did not predict ignition while a Chapman-Jouguet detonation wave was observed in the experiments for even smaller pressure ratios. Here we have shown that sound wave perturbations can cause large reductions in ignition times. For example, a perturbation of amplitude 200m/s and half-wavelength of 90cm causes ignition as early as 660μs which is sufficient to explain the discrepancy between the numerical predictions and the experimental observations.

V. CONCLUSIONS

In this paper detailed numerical simulations of incident shock tube experiments have been used first to verify earlier experimental observations[5,7] that a minimum power, a minimum energy and some relation between them is required to characterize the direct initiation of detonations. However, in the course of this study it became necessary to reconcile the quantitative differences between the numerical predictions and the experimental observations. This in turn led us to investigate the sensitivity of the mixtures in the region behind the incident shock to fluctuations in pressure and temperature which might cause early ignition in an experiment.

Simulations were carried out to evaluate the effects of sound wave perturbations which in turn result in temperature and pressure fluctuations. The results of these sound wave studies shows how the ignition time is affected by sound waves of a given amplitude and frequency. We note that low frequency perturbations (~480 Hz or half wavelength L ~ 75 cm) of large enough amplitude (~200 m/s) can reduce the ignition time by an order of magnitude. We also observe that low frequency perturbations are more likely than high frequency perturbations to cause the observed discrepancies between the experiments and the calculations.

The presence of temperature and pressure variations in the experiments can be due to factors such as the non-ideal

break-up of the diaphragm, boundary layers causing non-uniformities in the walls of the tube, the sudden change in shape and area of cross-section between the driver and driven sections, or heat loss to the walls. However, perturbations required to substantially alter the ignition times to cause such discrepancies as observed here may be larger than what might normally be present in very well controlled shock tube experiments. This needs to be investigated before one can confidently use shock tube studies to determine the critical conditions necessary to characterize the direct initiation of detonations.

Different systems will have different temperature, pressure, sound wave or other perturbations and we have shown here that such perturbations can substantially reduce the ignition time and hence the critical conditions. It appears that the critical conditions obtained from different experimental configurations will be different from each other and from practical systems. Therefore, further work needs to be done to estimate the perturbations likely to occur in various systems.

ACKNOWLEDGMENTS

The authors would like to acknowledge the help and encouragement of Drs. Homer Carhart and John Gardner in preparing this work. This research has been sponsored by the Office of Naval Research and the Naval Material Command.

REFERENCES

1. Zeldovich, Y.B., Kogarko, S.M. and Simonov, N.N.: Soviet Phys.-JETP 1, 1689 (1956).
2. Litchfield, E.L., Hay, M.H. and Forshey, D.R.: Ninth Symposium (International) on Combustion, p. 282, Academic Press, 1963.
3. Freiwald, H. and Koch, H.W.: Ninth Symposium (International) on Combustion, p. 275, Academic Press, 1963.
4. Bach, G.G., Knystautas, R. and Lee, J.H.: Thirteenth Symposium (International) on Combustion, p. 1097, The Combustion Institute, 1971.
5. Lee, J.H., Knystautas, R. and Guirao, C.M.: Fifteenth Symposium (International) on Combustion, p. 53, The Combustion Institute, 1975.
6. Knystautas, R. and Lee, J.H.: Combust. Flame. 27, 221 (1976).
7. Dabora, E.K.: Effect of Additives on the Lean Detonation Limit of Kerosene Sprays. UCONN0507-129-F, The University of Connecticut, 1980.
8. Oran, E.S., Young, T.R., Boris, J.P., and Cohen, A.: Weak and Strong Ignition-I. Naval Research Laboratory Memorandum Report 4664, 1981. (To appear in Combust. Flame).
9. Oran, E.S. and Boris, J.P.: Weak and Strong Ignition-II. Naval Research Laboratory Memorandum Report 4671, 1981. (To appear in Combust. Flame).

10. Oran, E.S., Young, T.R., and Boris, J.P.: Seventeenth Symposium (International) on Combustion, p. 43, The Combustion Institute, 1979.

11. Oran, E.S., and Boris, J.P.: Prog. Energy Combust. Sci. 7, 1 (1981).

12. Williams, F.A.: Combustion Theory, p. 2, Addison-Wesley, 1965.

13. Boris, J.P. and Book, D.L.: Methods in Computational Physics, Vol. 16, p. 85, Academic Press, 1976.

14. Boris, J.P.: Flux-Corrected Transport Modules for Solving Generalized Continuity Equations. Naval Research Laboratory Memorandum Report 3237, 1976.

15. Young, T.R., and Boris, J.P.: J. Phys. Chem. 81, 2424 (1977).

16. Young, T.R.: CHEMEQ, A Subroutine for Solving Stiff Ordinary Differential Equations. Naval Research Laboratory Memorandum Report 4091, 1980.

17. Burks, T.L., and Oran, E.S.: A Computational Study of the Chemical Kinetics of Hydrogen Combustion. Naval Research Laboratory Memorandum Report 4446, 1980.

18. Stull, D.R., and Prophet, H.: JANAF Thermochemical Tables, 2nd edition, Nat. Stand. Ref. Data Serv., Nat. Bur. Stand., No. 37, 1971.

19. Edelson, D.: Science. 214, 981 (1981).

FIGURE CAPTIONS

Figure 1. Time history of (a) the shock velocity, (b) the contact surface velocity, and (c) the pressure behind the shock front for the diaphragm pressure ratio of 110.

Figure 2. Time history of (a) the shock or detonation velocity, (b) the contact surface velocity, and (c) the pressure behind the shock front for the diaphragm pressure ratio of 150. The Chapman-Jouguet detonation velocity is 2 km/s.

Figure 3. Time history of the power and energy for the diaphragm pressure ratio of (A) 110 and (B) 150.

Figure 4. The pressure ratios and the corresponding detonation locations observed in the experiments and in the numerical simulations. M is the initial Mach number of the shock.

Figure 5. Time history of the temperature at three locations in a 0.9m long system with the sound wave perturbation of amplitude 100 m/s.

Figure 6. The ignition time as a function of the amplitude of the sound wave perturbation in systems of various length.

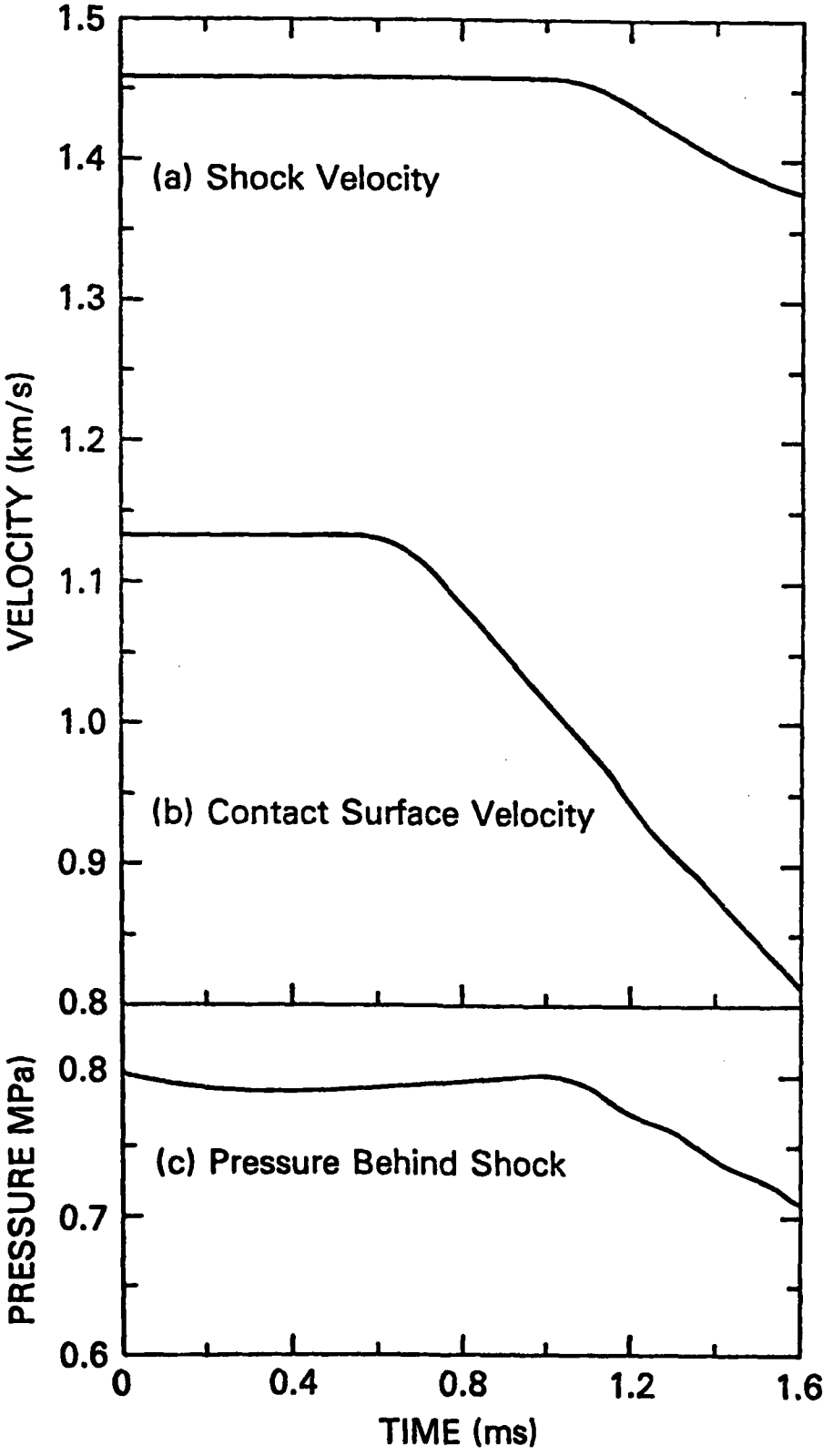
1.5
1.4
(a) Shock Velocity
1.3
1.2
1.1
1.0
(b) Contact Surface Velocity
0.9
0.8
VELOCITY (km/s)
0.8
0.7
0.6
(c) Pressure Behind Shock
PRESSURE MPa)
0
0.4
0.8
1.2
1.6
TIME (ms)

Figure 1

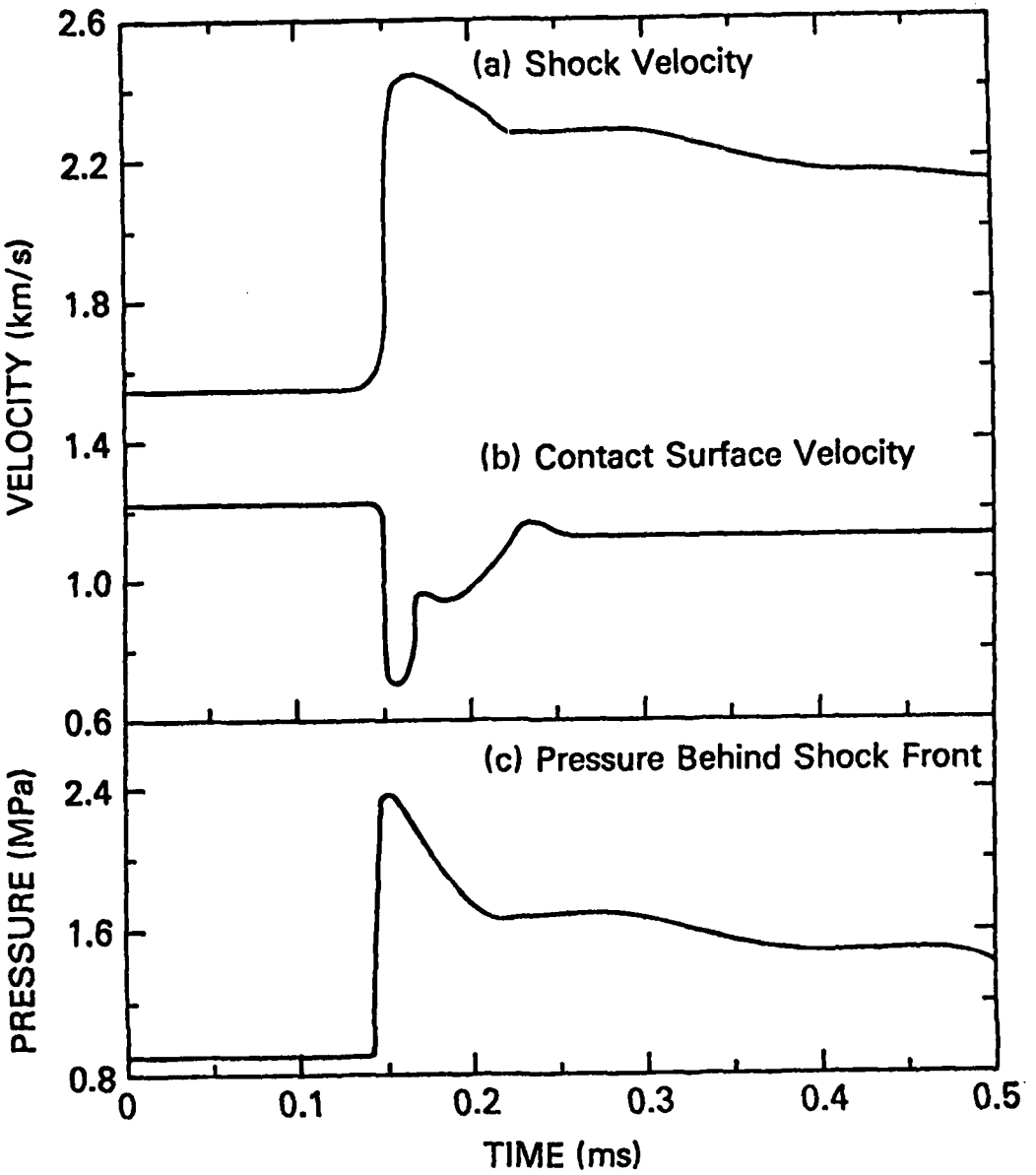
(a) Shock Velocity
(b) Contact Surface Velocity
(c) Pressure Behind Shock Front
VELOCITY (km/s)
PRESSURE (MPa)
TIME (ms)
2.6
2.2
1.8
1.4
1.0
0.6
2.4
1.6
0.8
0
0.1
0.2
0.3
0.4
0.5

Figure 2

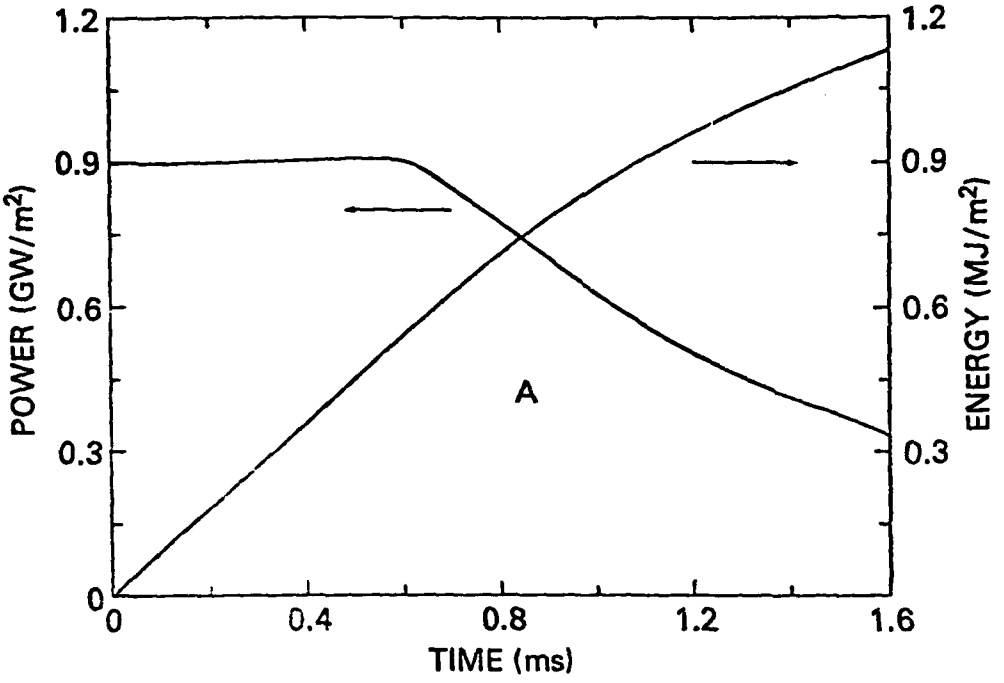
1.2
0.9
0.6
0.3
0
POWER (GW/m²)
ENERGY (MJ/m²)
A
0
0.4
0.8
1.2
1.6
TIME (ms)

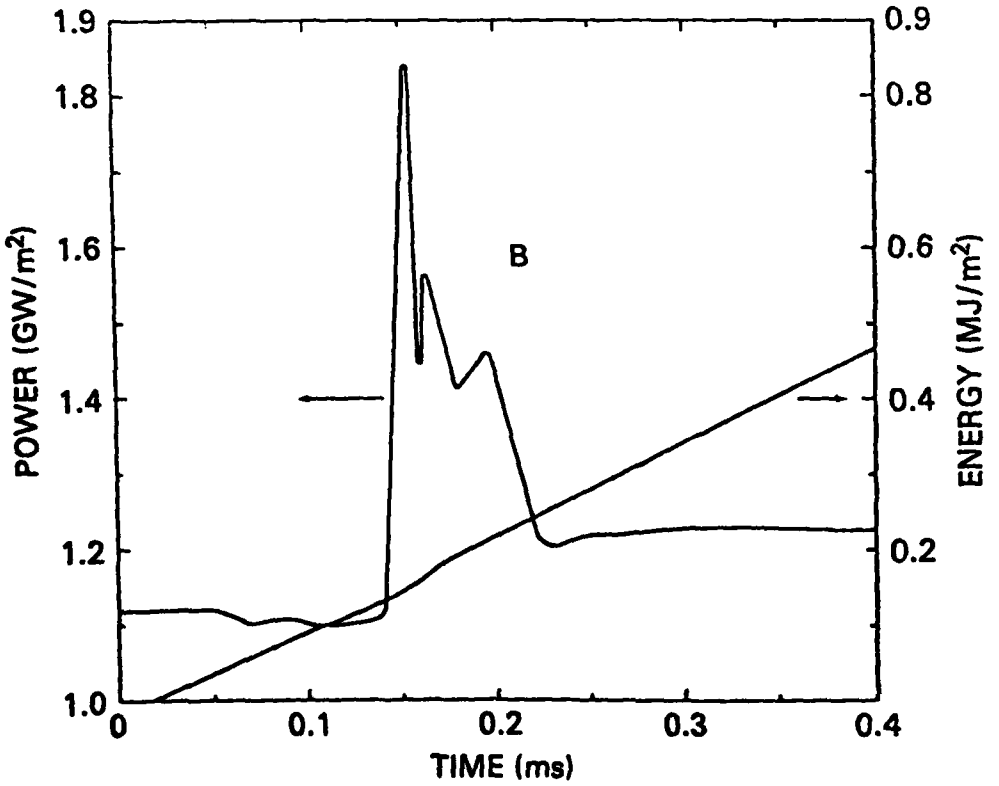
1.9
1.8
1.6
1.4
1.2
1.0
0.9
0.8
0.6
0.4
0.2
POWER (GW/m²)
ENERGY (MJ/m²)
B
0
0.1
0.2
0.3
0.4
TIME (ms)

Figure 3

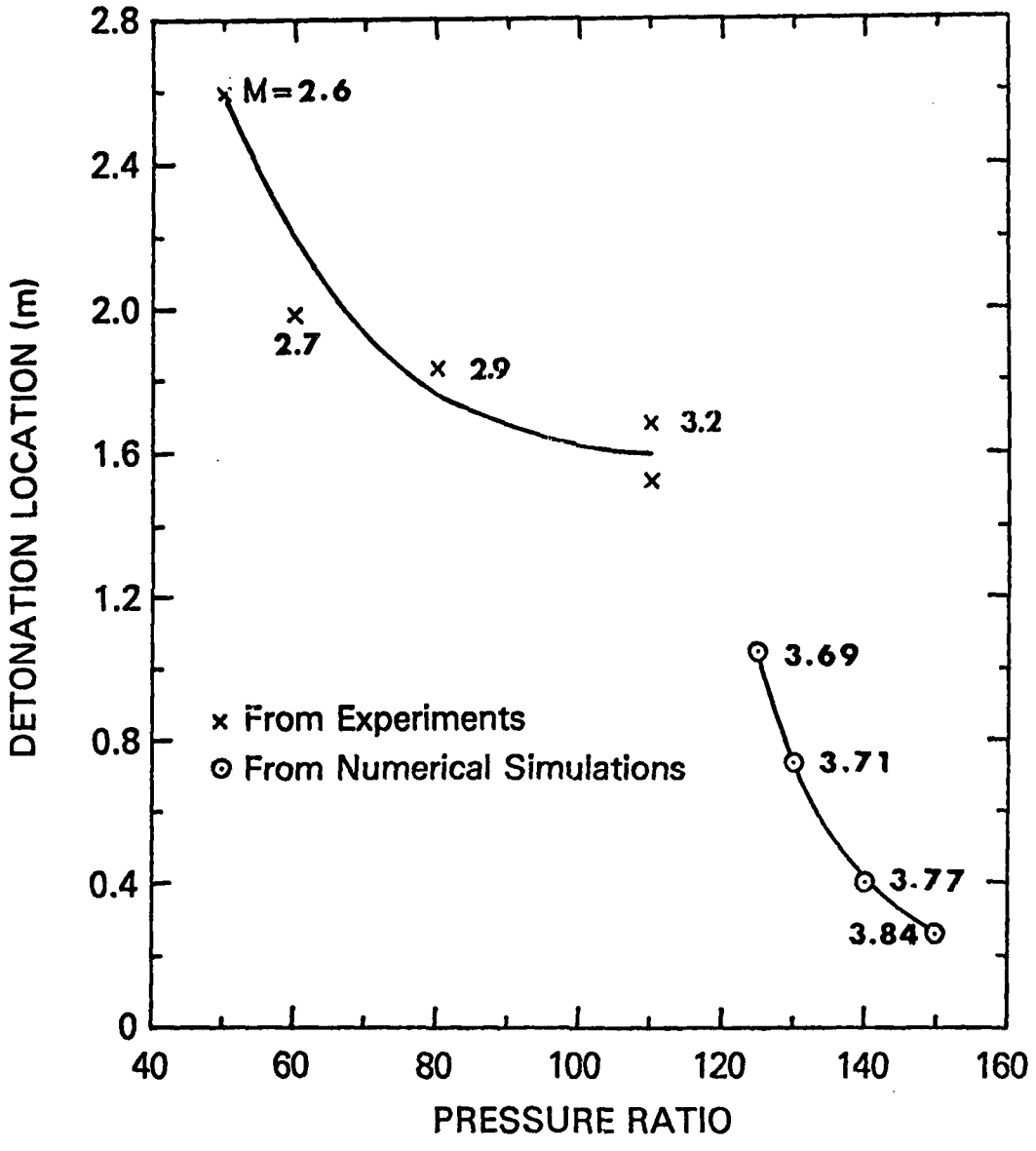
DETONATION LOCATION (m)
PRESSURE RATIO
2.8
2.4
2.0
1.6
1.2
0.8
0.4
0
40
60
80
100
120
140
160
M=2.6
2.7
2.9
3.2
3.69
3.71
3.77
3.84
× From Experiments
⊙ From Numerical Simulations

Figure 4

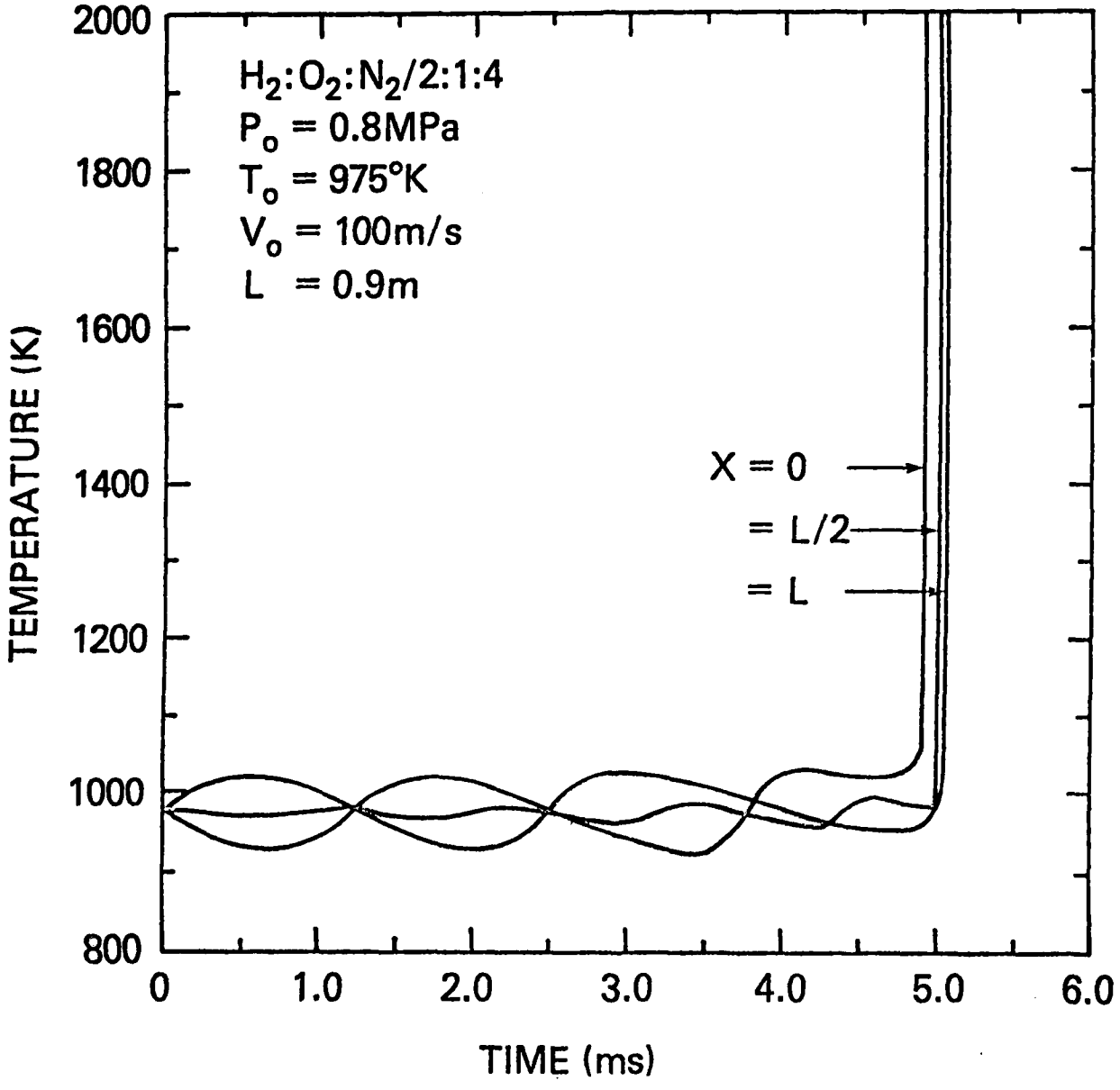
2000
1800
1600
1400
1200
1000
800
TEMPERATURE (K)
$H_2:O_2:N_2/2:1:4$
P_o = 0.8MPa
T_o = 975°K
V_o = 100m/s
L = 0.9m
X = 0
= L/2
= L
0
1.0
2.0
3.0
4.0
5.0
6.0
TIME (ms)

Figure 5

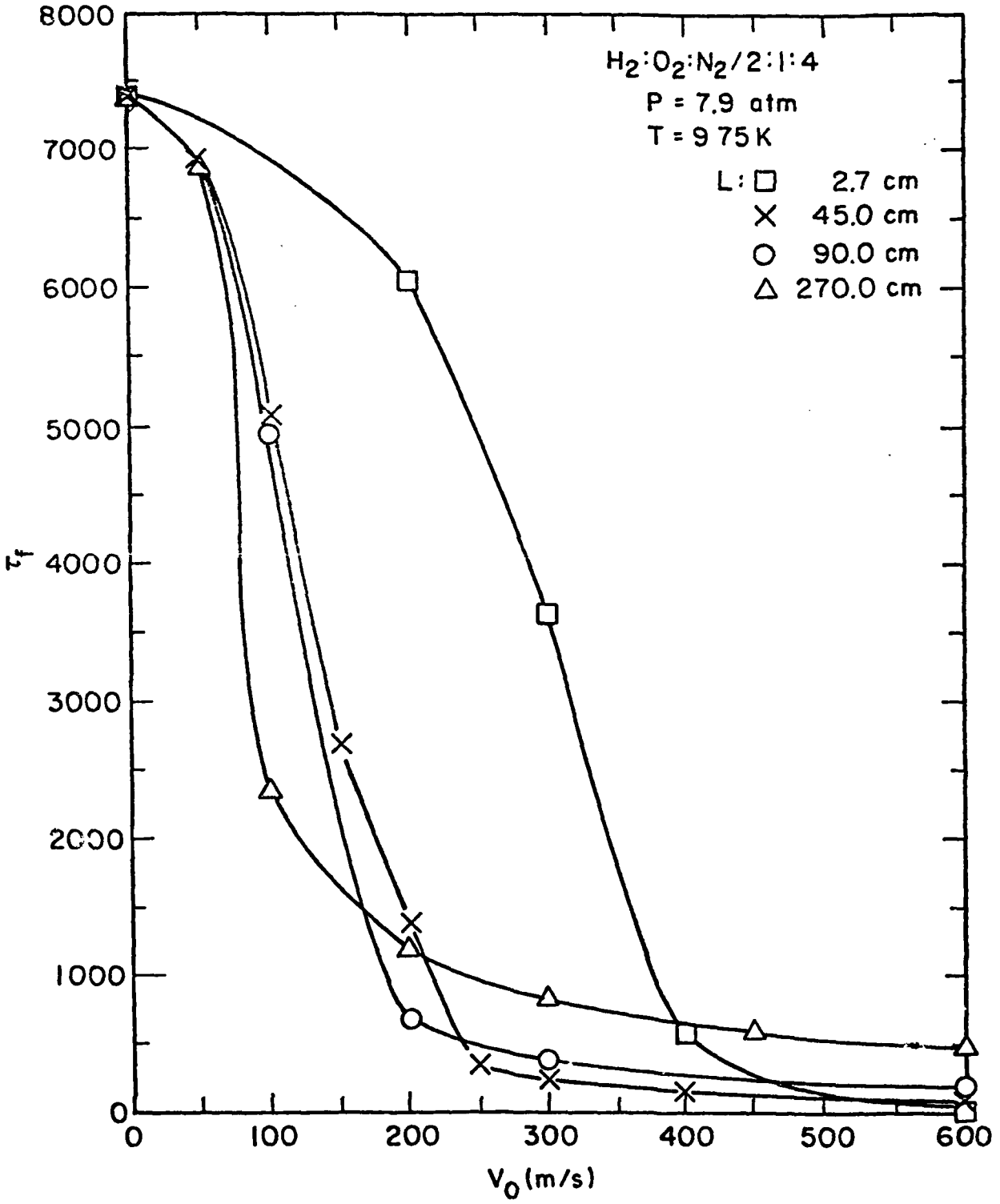
8000
7000
6000
5000
4000
3000
2000
1000
0
τ_i
0
100
200
300
400
500
600
V_0 (m/s)
$H_2:O_2:N_2/2:1:4$
P = 7.9 atm
T = 975 K
L: 2.7 cm
45.0 cm
90.0 cm
270.0 cm

Figure 6

END

DATE
FILMED

10-82

DTIC